Detection of the missing cascaded Magneto-Chiral Anisotropy

José M. Caridad[1,2,3], Christos Tserkezis[4], Jaime E. Santos[5], Paulina Plochocka[6], M. Venkatesan[1], J.M.D. Coey[1], N. Asger Mortensen[3,4,7], Geert L.J.A. Rikken[6] and Vojislav Krstić[1,8]

[1]*School of Physics, CRANN, Amber Research Centre, Trinity College Dublin, College Green, Dublin 2, Ireland*

[2]*DTU Physics, Technical University of Denmark, 2800 Kongens Lyngby, Denmark*

[3]*Center for Nanostructured Graphene, Technical University of Denmark, 2800 Kongens Lyngby, Denmark*

[4]*Center for Nano Optics, University of Southern Denmark, Campusvej 55 DK-5230 Odense, Denmark*

[5]*Centro de Física, Universidade do Minho, P-4710-057 Braga, Portugal*

[6]*Laboratoire National des Champs Magnétiques Intenses, UPR3228 CNRS/INSA/UGA/UPS, Toulouse and Grenoble, France*

[7]*Danish Institute for Advanced Study, University of Southern Denmark, Campusvej 55 DK-5230 Odense, Denmark*

[8]*Department of Physics, Friedrich-Alexander-University Erlangen-Nürnberg (FAU), Staudtstr. 7, 91058 Erlangen, Germany*

Being the intimate connection between chirality and magnetism, magneto-chiral anisotropies (MChA) - featuring non-reciprocal optical responses in chiral systems depending on the relative direction of the magnetic field *B* and the light propagation -

have attracted much attention throughout the recent history of science[1-3]. The genuine two[4-9] MChA phenomena are the so-called 'pure'[4-6,9] and 'cascaded'[7-9] effects. The 'pure' MChA phenomenon is proportional to the relative orientation between the wave vector of light *k* and *B* and has already been verified in numerous materials[10-16] after its first observation in the late 20th century[10]. In marked contrast, the predicted 'cascaded' MChA effect remains unrevealed[8,9,14]. This intriguing 'cascaded' form of MChA is given by the simultaneous action of natural and magnetically induced optical activities in chiral systems and is the hallmark of bianisotropic electromagnetic materials generally referred to as Faraday chiral media[17-21].

Here, we report on the experimental observation of the elusive cascaded MChA and demonstrate its enantioselectivity. Corresponding electromagnetic simulations are in remarkable quantitative agreement with our measurements, which demonstrates the controllability of this phenomenon. The existence of this exotic effect is crucial in light-matter interactions, molecular spectroscopy and the design of novel metamaterials.

KEYWORDS cascaded Magneto-Chiral Dichroism, photonic crystals, chiral nanomagnets, Faraday Chiral media, Metasurfaces, complex electromagnetic media

The interplay between electromagnetism and chirality possesses a rich and long history, comprising cornerstone discoveries that have largely contributed to our understanding of the electromagnetic properties of matter and the wave nature of light.[1-3] The exploration of this interdisciplinary field was initiated during the 19th century, when Arago discovered the natural optical activity (NOA), a non-local response in media that lack mirror symmetry (chiral systems). [1-3] Later, Faraday detected magnetically induced optical activity (MOA), an omnipresent phenomenon resulting from the breaking of the time-reversal symmetry by a

magnetic field perpendicular to the optical polarization.[1-3] Despite their different physical roots, NOA and MOA are both manifested in a different absorption/emission (dichroism) or refraction (birefringence) between left and right circularly polarized light. Such phenomenological resemblances inspired several scientists, including Pasteur[1,2], to search for possible links between chirality and magnetism.

The late 20th century was a prolific time in the quest for optical responses connecting both chirality and magnetism, sparked first by a renaissance of interest on the topic at a theoretical level.[4-9] Based on symmetry arguments, Baranova and Zeldovich[4] deduced a second-order contribution (quantified by a parameter γ) with a dependence $\boldsymbol{k}\cdot\boldsymbol{B}$ to the dielectric constant of a chiral medium subjected to a magnetic field (Methods), possessing opposite sign for the two enantiomers of the chiral medium. Regarded as a magnetically induced change of NOA in the chiral medium, the appearance of this $\boldsymbol{k}\cdot\boldsymbol{B}$ dependence was underpinned by Wagnière *et al.*[5] and Barron *et al.*[6] by using formalisms from molecular theory. They referred to this effect as 'magneto-chiral anisotropy' (MChA), using the specific terminology 'magneto-chiral dichroism' in absorption or emission, and 'magneto-chiral birefringence' in refraction, in analogy with NOA and MOA.

Eritsyan[7,8] envisioned a conceptually-different MChA effect by only assuming a linear expansion of the dielectric constant expanded in terms of k and B (Methods). This MChA phenomenon is related to materials exhibiting NOA (quantified by a parameter α) and MOA (quantified by a parameter β) at concurring wavelengths and is coined 'cascaded' effect, proportional to the product of the coefficients $\alpha\beta$. The existence of the cascaded MChA phenomenon was independently predicted by Rikken and Raupach[9]. Intriguingly, despite being broadly predicted[7-9,17-22] and sought after[9,14], the observation of this 'cascaded' form of MChA has not been unveiled. This is surprising for two reasons: *i)* since its first observation in 1997[10], the 'pure' MChA counterpart has been detected in several chiral systems[9-16] and measurement

configurations including absorption[9], emission[10], photochemistry[13] or refraction[14,15] ; and *ii)* being MOA ubiquitous, media exhibiting the pure phenomenon also display NOA and should therefore show the cascaded MChA effect, too.

This oddity can be resolved emphasizing that selected chiral systems with large NOA and MOA responses at coincident wavelengths are required to detect the cascaded MChA.[10,14] Specifically, the magneto-optical response of *biaxial chiral systems* such as artificial ferromagnetic helical nanostructures is expected to be governed by the cascaded phenomenon.[8,17-21] Moreover, cascaded and pure MChA effects in these systems exhibit distinctly different scattering anisotropy behaviour. In transmission, the pure effect shows a maximum at the NOA resonance[14,21]; whereas the cascaded phenomenon is predicted to exhibit a distinct zero-crossing at the NOA resonance instead[14,21].

Further insight on the anisotropy of light scattering in ferromagnetic helical media can be gained by considering the case of normal reflection. One can demonstrate,[21] that the anisotropy in reflection in this media stems from an unconventional odd-powered term of cascaded form

$$\Delta = \alpha\beta \boldsymbol{k} \cdot \boldsymbol{B} \qquad \text{(Eq. 1)}$$

appearing in the (quartic) dispersion relation of the system (details in Supplementary Note 1). Notably, the presence of this odd-powered term makes each dispersion relation solution to be of the form[8] $\boldsymbol{k} \approx \boldsymbol{k}_0 \pm a_0 \alpha\beta |\boldsymbol{B}|$, where $\boldsymbol{k}_0$ is the wavevector for zero α or β, and a_0 is a constant (Supplementary Note 1). Therefore, $\boldsymbol{k}$ has different magnitudes for forward and backward propagation[8,21]. Only at the NOA resonance, $\boldsymbol{k}$ possesses identical magnitude for forward and backward propagation, which (similar to the transmission case) gives rise to a zero-crossing in the reflection anisotropy. In other words, light propagation is reciprocal at this wavelength.[8,14,21] We emphasise that none of these distinct features are present in helical systems if $\beta = 0$, regardless of the presence or not of the pure MChA γ. Specifically, if $\gamma \neq 0$; and $\beta = 0$, chiral systems with helical structure show a reciprocal response at fixed $\boldsymbol{B}$. As such,

the magnitude of *k* is the same for forward and backward propagation at any wavelength, which implies a vanishing pure MChA in reflection.

By taking into account these premises, we demonstrate here the univocal detection of the cascaded MChA phenomenon in the normally reflected magneto-optical signal of nickel helical nanostructures[22] (Figure 1a). Contrary to naturally gyrotropic systems[9-15], NOA in artificial helical media is exclusively caused by the twisting of the medium[7,8,21,28]. Also, the enhanced MOA in these nanostructures is primarily due to the use of a ferromagnetic material[21,29].

Figure 1b depicts the specific experimental set-up (Methods) used here to measure the cascaded MChA effect in ferromagnetic nanohelices in reflection. We use light from a laser source as the incident radiation and, to increase sensitivity, the magnetic field is alternated in the two opposite configurations ($\pm|\boldsymbol{B}|$) so the reflectance difference $\Delta R = R(+|\boldsymbol{B}|) - R(-|\boldsymbol{B}|)$ is measured with a phase-sensitive detection method. Factors related to excitation intensity and sample geometry are eliminated by dividing ΔR by the total, static reflectance signal $R(0)$. Therefore, the resulting quantity $\Delta R / R(0)$ normalized by $|\boldsymbol{B}|$ corresponds to the cascaded MChA factor η (governing contribution in these systems in reflection[21], see Supplementary Note 1):

$$\eta = \left(\Delta R / R(0)\right)|\boldsymbol{B}|^{-1} \quad \text{(Eq. 2)}$$

We have fabricated[23-27] (Methods) regular arrays of artificial nickel nanohelices with ~1 turn and a pitch p of ~320 nm (Figure 1c) in both types of enantiomer -right-handed (RH) and left-handed (LH) helices- as our specific ferromagnetic (Supplementary Note 2) chiral medium.

Figure 2a shows the measured reflectance difference at zero *B* field between right- and left-handed circular polarized light, $R^{RHCP} - R^{LHCP}$ in both RH and LH helices. This signal is a manifestation of the NOA of the system and exhibits a relatively broad response with a maximum of magnitude (~0.3) at a wavelength $\lambda^{\max}$ ~640 nm for both enantiomers.

Figure 2b shows the measured $\eta(\lambda)$ plotted for the two enantiomers of the helical structure under study in the wavelength range 440 to 740 nm and at $|\boldsymbol{B}|$ = 0.375 T. $\eta(\lambda)$ shows opposite behaviour in both RH and LH enantiomers with similar magnitudes. Also, its magnitude increases when increasing $|\boldsymbol{B}|$ (Supplementary Note 4). Strikingly, we observe a zero-crossing of $\eta(\lambda)$ occurring at ~633 nm, position very close to λ^{max} (NOA maximum) and with a non-zero MOA (Supplementary Note 5). $\eta(\lambda)$ changes sign at the two opposite sides of λ^{max} of this crossing in both enantiomers. As aforementioned, the latter two findings are the unique hallmarks of the predicted cascaded MChA phenomenon[8,9,21] and thus demonstrate its detection. The magnitude of the dissymmetry factor η is ~10^{-5} T^{-1}, which is in good agreement to the common assumption[9,14,16] given by the product of NOA and MOA (independently measured) in our samples: α ~0.3 (Figure 2a) and β ~10^{-4} T^{-1} (Supplementary Note 5).

We additionally corroborate the observation of the cascaded MChA by undertaking advanced electromagnetic simulations (Methods), calculating the expected magneto-optical response of our nickel nanohelices in normal reflection. In these calculations, NOA is implicitly considered by the helical shape of the structures and MOA is included in the system by accounting for the permittivity tensor of the ferromagnetic material (nickel) in the presence of a magnetic field[30]. Figure 3a shows the calculated reflectance difference at zero *B*, $R^{RHCP} - R^{LHCP}$, exhibiting a broad response[23,28] with a maximum (~0.3) at a wavelength λ^{max} ~665 nm for both enantiomers. Thus, these features as well as the overall line-shape are in good agreement with the NOA response measured in our nanohelices (Figure 2a).

Figure 3b depicts the calculated $\eta(\lambda)$ for the two enantiomers of the chiral system under study. $\eta(\lambda)$ exhibits a zero-crossing occurring at the NOA resonance (~650 ± 25 nm) and with opposite sign of the slope for each enantiomer. The magnitude found for $\eta(\lambda)$ at these

wavelengths is ~10^{-5} T^{-1}. Remarkably, both line shape and magnitude of the calculated $\eta(\lambda)$ are in excellent quantitative agreement with our experiments (Figure 2b), especially when considering that no theory has been able to model successfully any MChA effect up to date[9-16]. For completeness (Supplementary Note 3), we further calculate the normalized total transmission difference $\tau(\lambda)$ of our ferromagnetic nanohelices. $\tau(\lambda)$ does not show any zero-crossing close to λ^{max} (< ±25 nm) since it entails more contributions than just the cascaded MChA[14,16,21]. This calculation reconfirms normal reflection as unique measurement to unambiguously detect the cascaded MChA in ferromagnetic nanohelices[21].

In conclusion, we have reported the detection of the long missing cascaded form of MChA. This effect is perceptible in the normal reflectance difference from ferromagnetic helical nanostructures, samples and measurement configuration appropriately designed so that this magneto-optical effect is dominant. The existence of the cascaded MChA fully validates the phenomenological electromagnetic constructs utilized to conceptualize magneto-chiral effects[4-9,17-21]. This phenomenon opens the door to the observation of exotic wave properties predicted to occur in Faraday chiral media[17-22] such as negative reflection[19] and the realization of envisioned electromagnetic devices like optical diodes[21].

Figures

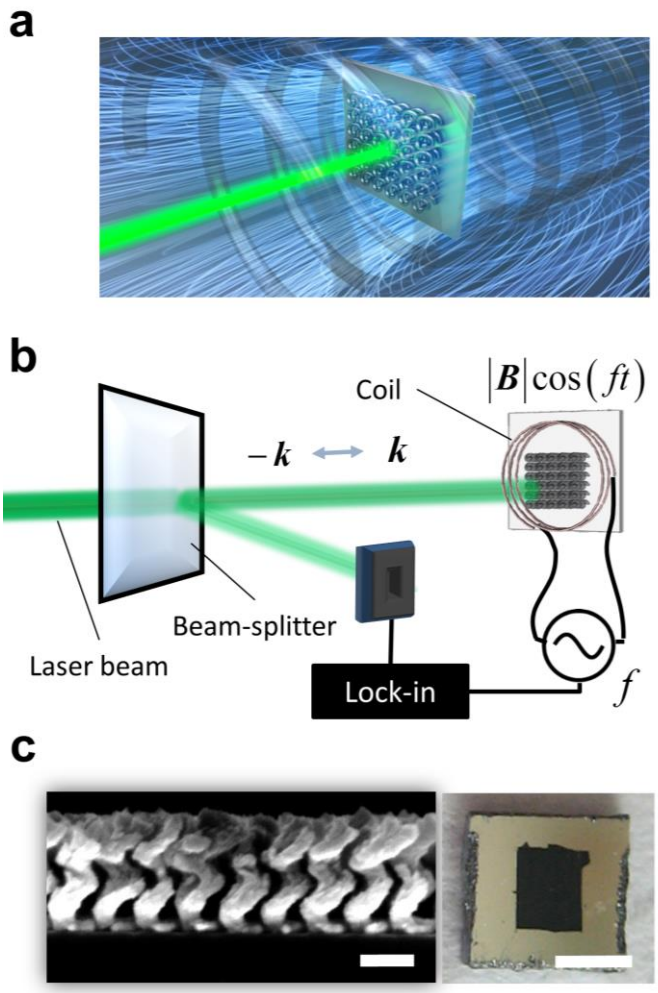

Figure 1. Detection of cascaded MChA in periodic arrays of nanohelices. a, Illustration of the study. Arrays of ferromagnetic nanohelices are subjected to the external magnetic field *B* generated by a coil, collinear to their helical axis. Samples are excited (brighter green) with linearly polarized light which propagates parallel to the helical axis, too. The normally reflected magneto-optical signal from the sample (darker green) is proportional to the cascaded MChA effect[21], allowing its experimental detection as shown below. **b**, Schematic of the experimental set-up. The external magnetic field *B* is generated by a coil and is collinear with the propagation direction and the helical axis. Samples are excited with linearly polarized light at four different laser wavelengths (440 nm, 540 nm, 633 nm and 741 nm). The optical reflectance from the sample is detected by a silicon photodiode (PD). The intensity difference (ΔR) between the

two magnetic field directions is phase-sensitively detected by a lock-in amplifier at the frequency f=19 Hz of the alternating magnetic field. **c**, (Right panel) optical image showing the array of ferromagnetic (nickel) nanohelices on top a 80 nm thick silver film. Scale bar is 1 mm. (Left panel) scanning electron micrograph of one of the enantiomers, showing well defined nickel nanohelices with a pitch of ~320 nm . Scale bar is 300 nm.

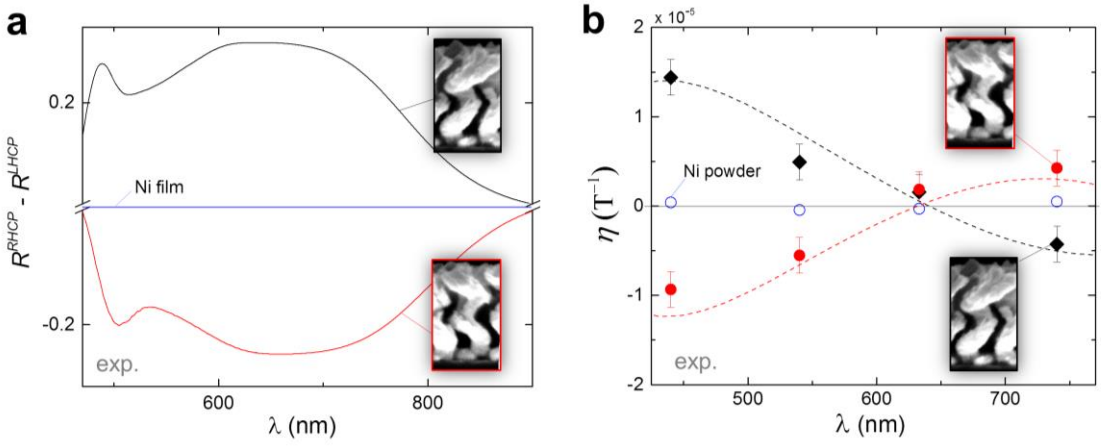

Figure 2. Experimental MChA in ferromagnetic helices in reflection. a, NOA of our samples measured as the normal reflectance difference $R^{RHCP} - R^{LHCP}$ between right- and left-handed circular polarized light in RH (black) and LH (red) helices at zero magnetic field. Both enantiomers show a clear maximum ~0.3 which appears within a region around ~640 nm. A zero reflectance difference is measured for a thin film of nickel (blue). **b** cascaded MChA signal in reflection η for both RH (black) and LH (red) helices plotted as a function of the used laser wavelengths, exhibiting zero-crossing close to the NOA maximum and a change of sign at both sides of this position in each enantiomer[8,14]. These measurements are undertaken with linearly polarized light in an external magnetic field $|\boldsymbol{B}|$ = 0.375 T. Dashed lines are only meant to guide the eye. For reference, a η below 5×10^{-7} T^{-1} was measured at any wavelength for nickel powder (blue circles), indicating the detection limit in our setup.

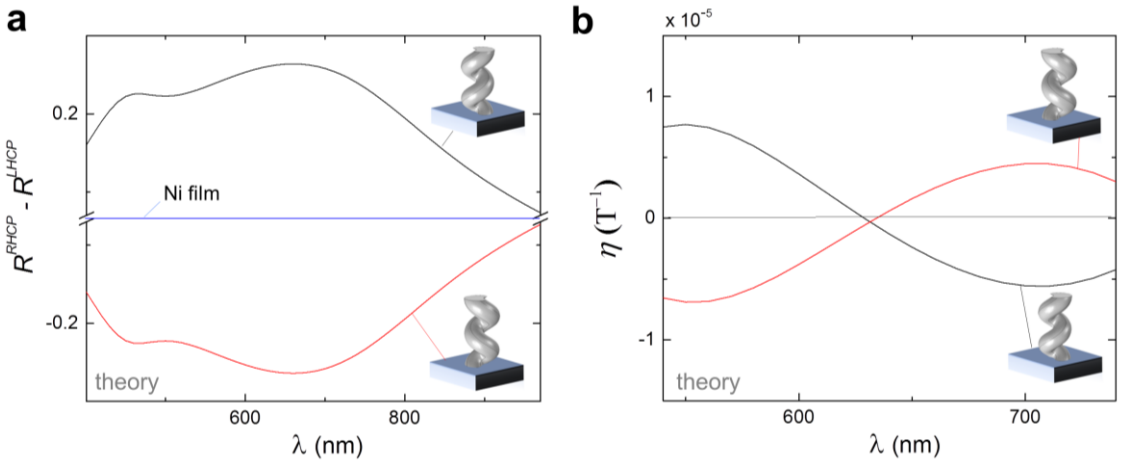

Figure 3. Calculated MChA in ferromagnetic (nickel) nanohelices placed on a silver substrate in reflection. a, NOA. Calculated reflectance difference between righ- (R^{RHCP}) and left- (R^{LHCP}) handed circular polarized light in RH (black) and LH (red) helices and a nickel film (blue) at zero magnetic field. The NOA maximum appears within the range of 550 to 770 nm. **b** , calculated MChA signal η in normal reflection of both RH (black) and LH (red) helices plotted as a function of the wavelength λ , exhibiting a clear cascaded MChA behaviour in ferromagnetic nanohelices, similar to the one predicted for helical media[8,14,21] (zero-crossing close to NOA maximum and corresponding sign change for both enantiomers). These calculations are undertaken with linearly polarized light (as in the experiment).

Methods

Dielectric function ε in chiral media: pure and cascaded MChA phenomena

Optical magneto-chiral effects can be formalized by expanding the dielectric tensor of chiral media subject to a magnetic field to first order in both the magnitude of the wave vector of the incoming radiation ($\boldsymbol{k}$) and the magnitude of the total magnetic field ($\boldsymbol{B}$) within the chiral

media[4-6,9]. Here, we discuss the form of the dielectric tensor for two common type of media: homogeneous and periodic arrays of nanohelices (our samples in consideration).

A. Dielectric function in homogeneous media, including uniaxial crystals with optical axis collinear to $\boldsymbol{k}$, $\boldsymbol{B}$

Homogeneous and isotropic media (or uniaxial crystals with their optical axis collinear to $\boldsymbol{k}$, $\boldsymbol{B}$ and the helical axis), lead to a complex dielectric tensor for the ± circular eigenmodes[9]:

$$\varepsilon_{\pm}(\omega,\boldsymbol{k},\boldsymbol{B}) = \varepsilon(\omega) \pm \alpha^{d/l}(\omega)\boldsymbol{k} \pm \beta(\omega)\boldsymbol{B} + \gamma^{d/l}(\omega)\boldsymbol{k}\cdot\boldsymbol{B}, \quad \text{(Eq. 3)}$$

where $\varepsilon(\omega)$ is the permittivity at zero field, the coefficients $\alpha^{d/l}(\omega)$ and $\beta(\omega)$ represent NOA and MOA, respectively, and $\gamma^{d/l}(\omega)$ refers to the pure MChA effects for right- (d) and left- (l) handed media. We note that under parity transformation $\hat{P}\gamma^{d}(\omega) = -\gamma^{d}(\omega) = \gamma^{l}(\omega)$ and $\hat{P}\alpha^{d}(\omega) = -\alpha^{d}(\omega) = \alpha^{l}(\omega)$. We have omitted the super indices (*d*, *l*) and the frequency dependence ω for all coefficients in the main text for simplicity.

Eq. 3 clearly shows that the pure MChA depends on the relative orientation of these two vectors ($\boldsymbol{kB} = |\boldsymbol{k}||\boldsymbol{B}|\cos\theta$, with θ being the angle between $\boldsymbol{k}$ and $\boldsymbol{B}$).

B. Dielectric function for periodic arrays of nanohelices

Artificial helical nanostructures, such as the here considered ferromagnetic nanohelices, are periodically inhomogeneous media with biaxial dielectric permittivity[21,31]. In the presence of a magnetic field $\boldsymbol{B}$ directed along the helical axis, and considering only a linear expansion, Eritsyan[8] and Gevorgyan[21] showed that the dielectric constant in these systems is a tensor that can be expressed as:

$$\varepsilon(z)=\varepsilon_m\cdot\begin{pmatrix} 1+\delta_\varepsilon\cos(2az) & \delta_\varepsilon\sin(2az)+\dfrac{i\beta|\boldsymbol{B}|\cos\theta}{\varepsilon_m} & 0 \\ \delta_\varepsilon\sin(2az)-\dfrac{i\beta|\boldsymbol{B}|\cos\theta}{\varepsilon_m} & 1-\delta_\varepsilon\cos(2az) & 0 \\ 0 & 0 & 1-\delta_\varepsilon \end{pmatrix} \quad \text{(Eq. 4)}$$

where $\varepsilon_m=(\varepsilon_1+\varepsilon_2)/2$, $\delta_\varepsilon=(\varepsilon_1-\varepsilon_2)/(\varepsilon_1+\varepsilon_2)$ and $\varepsilon_1,\varepsilon_2$ are the principal axis of the dielectric constant tensor in a coordinate frame (local to the structure) that rotates with respect to the Cartesian laboratory coordinate frame (*x*,*y*,*z*), in the absence of magnetic field. We note that NOA in this artificial system[8,21,31] is exclusively caused by the twisting of the medium and is reflected in Eq.4 by the parameter $a=2\pi/p$, where *p* is the helical pitch.

Experimental setup to observe cascaded MChA effects

Figure 1b depicts the experimental set-up used to observe the cascaded MChA effect based on normal specular reflection. We use four laser sources (440, 540, 633 and 740 nm) and a phase-sensitive detection method using a lock-in amplifier at a frequency *f* = 19 Hz to detect the signal η. The main difference with respect to the one used for transmission measurements[14-16] is the inclusion of a beam splitter directing the normally reflected radiation towards the photodetector.

Fabrication of arrays of ferromagnetic metallic nanohelices

We have fabricated regular arrays of metal nanohelices of the two opposite enantiomers made from nickel using an oblique evaporation technique[23,25]. Our samples (Figure 1c) have an approximate pitch of 320 nm, a diameter of 160 nm and separated 200 nm from neighbouring

helices. They are grown on Si substrates with a ~ 100 nm thin film of silver evaporated on top, film which enables the creation of regular helices with a large (>200 nm) pitch[23].

Figure 1c, right panel shows a top-view optical image of the nickel nanohelix array of approx. size 1mm^2 (black square) on top of the Ag film. The matt-black appearance indicates a strong visible-light absorption in nickel nanohelices as demonstrated in our previous study[24]. Supplementary Note 2 shows the magnetization curve of these samples with external magnetic field applied parallel to the axis of the nanohelices. They show a clear ferromagnetic behaviour.

Numerical simulations

Finite-element method calculations were performed with the commercial software COMSOL 5.1. Nickel helices were arranged on a 200-nm thick silver substrate. Floquet periodic boundary conditions were used in the xy plane, while a 500 nm thick perfectly matched layer (PML) was used at the top (air) side of the geometry, and a scattering boundary condition at the bottom (silver) side. To achieve the desired spacing between helices of 200 nm, the one helix contained in the unit cell was divided in smaller parts centred around the unit cell edges (see Supplementary Note 6). For the finite-element discretisation, a mesh of 108000 domain elements with maximum element size 20 nm and minimum element size 2 nm was found sufficient to provide converged spectra. The structure was illuminated by a plane wave (circularly or linearly polarised) impinging from the top side, and reflection (transmission) spectra were calculated by integrating energy flow over the entire top (bottom) faces (at the air-PML interface and the edge of the silver substrate, respectively). Silver was described by the dielectric function of Johnson and Christy[32], while nickel was described by a 3x3 tensor with a retarded Drude model with two extra Lorentzians as its diagonal components, and Lorentzian oscillator contributions for the off-diagonal elements[30]. Further information about these calculations can be found in the Supplementary Note 6. We emphasize that these

numerical simulations account for both pure and cascaded MChA contributions in our nickel nanohelices: NOA is present in the system due to the helical shape and MOA is included by accounting for the permittivity tensor of the material (nickel) in the presence of a static magnetic field[31].

References

1. L. D. Barron. Molecular light scattering and optical activity. *Cambridge University Press* (2004)
2. I.V. Lindell, A.H. Sihvola, S.A. Tretyakov and A.J. Viitanen. Electromagnetic waves in chiral and bi-isotropic media. *Artech House Inc*. (1994)
3. G. H. Wagnière. On chirality and the universal asymmetry: Reflections on image and mirror image. *John Wiley & Sons* (2008)
4. N.B. Baranova and B.Y. Zeldovich. Theory of a linear magnetorefractive effect in liquids. *Mol. Phys.* **38**, 1085 (1979)
5. G.H. Wagnière, A. Meier. The influence of a static magnetic field on the absorption coefficient of a chiral molecule. *Chem. Phys. Lett.* **93**, 78 (1982)
6. L.D. Barron and J. Vrbancich. Magneto-chiral birefringence and dichroism. *Molec. Phys*. **51**, 715 (1984)
7. O.S. Eritsyan. Optical problems in the electrodynamics of gyrotropic media. *Sov. Phys. Usp.* **25**, 919 (1982)
8. O.S.Eritsyan. Time dispersion, waves irreversibility and absorption effects in cholesteric liquid crystals. *Mol. Cryst. Liq. Cryst*. **348**, 79-99 (2000)
9. G.J.L.A. Rikken and E. Raupach. Pure and cascaded magnetochiral anisotropy in optical absorption. *Phys. Rev. E* **58**, 5081 (1998)

10. G.J.L.A. Rikken and E. Raupach. Observation of magneto-chiral dichroism. *Nature* **390**, 493 (1997)
11. C. Train, R. Gheorghe, V. Krstic, L.M. Chamoreau, N.S. Ovanesyan, G.J.L.A. Rikken, M. Gruselle and M. Verdaguer. Strong magneto-chiral dichroism in enantiopure chiral ferromagnets. *Nat. Mater*. **7**, 729 (2008)
12. R. Sessoli, M-E.Boulon, A. Caneschi, M. Mannini, L. Poggini, F. Wilhelm and A. Rogalev. Strong magneto-chiral dichroism in a paramagnetic molecular helix observed by hard X-rays. *Nat. Phys.* **11**, 69 (2014)
13. E. Raupach, G.L.J.A. Rikken, C. Train and B. Malézieux. Modelling of magneto-chiral enantioselective photochemistry. *Chem. Phys.* **261**, 373 (2000)
14. C.Koerdt, G. Düchs and G.L.J.A. Rikken. Magnetochiral anisotropy in Bragg scattering. *Phys. Rev. Lett*. **91**, 7, 073902 (2003)
15. P.Kleindienst, G.H. Wagnière. Interferometric detection of magnetochiral birefringence. *Chem. Phys. Lett*. **288**, 89 (1998)
16. S. Eslami, J.G. Gibbs, Y. Rechkemmer, J. v Slageren, M. Alarcón-Correa, T-C. Lee, A.G. Mark, G.L.J.A. Rikken and P. Fischer. Chiral nanomagnets. *ACS Photonics*, **1**, 1231 (2014)
17. N. Engheta and D.L. Jaggard. Electromagnetic Waves in Faraday chiral media. *IEEE Trans. Antennas and Propag*. **40**, 4, (1992)
18. W.S. Weilghofer and A. Lakhtakia. The correct constitutive relations of chiroplasmas and chiroferrites. *Microwave and Opt. Techno. Lett.* **17**, 6, 405 (1998)
19. T.G. Mackay and A. Lakhtakia. Negative reflection in a Faraday chiral medium. *Microwave and Opt. Techno. Lett.* **50**, 5, 1368 (2008)

20. I. Bita and E.L. Thomas. Structurally chiral photonic crystals with magneto-optic activity: indirect photonic bandgaps, negative refraction and superprism effects. *J. Opt. Soc. Am. B.* **22**, 6, 1199 (2005)
21. A.H. Gevorgyan and G.A. Vardanyan. Nonreciprocal reflection at the presence of absorption. Proc. SPIE 5218, Complex Mediums IV: Beyond Linear Isotropic Dielectrics, (9 July 2003); https://doi.org/10.1117/12.507791
22. A. Christofi and N. Stefanou. Strong magnetochiral dichroism of helical structures of garnet particles. *Optics Lett.* **15**, 38 4629 (2013)
23. J.M. Caridad, D. McCloskey, J.F. Donegan, V. Krstić. Controllable growth of metallic nanohelices at room temperature conditions. *Appl. Phys. Lett.* **105**, 233114 (2014).
24. J. M. Caridad, D. McCloskey, F. Rossella, V. Bellani, J.F. Donegan and V. Krstić. Effective Wavelength scaling of and damping in plasmonic helical antennae. *ACS Photonics* **2**, 675-679 (2015).
25. J.M. Caridad, S. Winters, D. McCloskey, G.S. Duesberg, J.F. Donegan, V. Krstić. Hot volumes as uniform and reproducible SERS-detection enhancers in weakly coupled metallic nanohelices. *Scientific Reports*, **7**, 45548 (2017).
26. J.J.Gough, D. McCloskey, J.M. Caridad, V. Krstić, M. Müller, N. Giaponik and A.L. Bradley. Chiral Ag nanostructure arrays as optical antennas. DOI: 10.1109/MetaMaterials.2015.7342532 (2015)
27. J.M. Caridad, S. Winters, D. McCloskey, G.S. Duesberg, J.F. Donegan and V. Krstić. Control of the plasmonic near-field in metallic nanohelices. Nanotechnology **29**, 32, 325204 (2018).

28. J.K. Gansel, M. Thiel, M. S. Rill, M. Decker, K. Bade, V. Saile, G. von Freymann, S. Linden and M. Wegener. Gold helix photonic metamaterial as broadband circular polarizer. Science **325**, 1513 (2009).
29. J.B. González-Díaz, A. García-Martín, G. Armelles, D. Navas, M. Vázquez, K. Nielsh, R.B. Wehrspohn and U. Gösele. Enhanced magneto-optics and size effects in ferromagnetic nanowire arrays. Adv. Mater. **19**, 18, 2643 (2007).
30. C. Wolff, R. Rodríguez-Oliveros and K. Busch. Simple magneto-optic transition metal models for time-domain simulations. Opt. Express **21**, 12022 (2013)
31. A. Lakhtaria and R. Messier, Sculptured Thin Films: Nanoengineered Morphology and Optics (SPIE, Washington, 2005)
32. P.B. Johnson and R.W. Christy. Optical constants of the noble metals. Phys.Rev. B **6**, 4370 (1972)

Acknowledgements

The authors want to thank A. Gevorgyan for useful comments and discussions. We thank the Advanced Microscopy Laboratory, CRANN, TCD for assistance during sample preparation. This work was supported by the Science Foundation Ireland contract-number PI-award 08/IN.1/I1873 and contract-number CSET 08/CE/I1432 and the European Union EuroMagNET II Programme. Part of this work was supported by the Cycle 4 of the Programme for Research in Third-Level Institutions (PRTLI4) Ireland. This work was supported by Programme Investissements d'Avenir under the program ANR-11-IDEX-0002-02, reference ANR-10-LABX-0037-NEXT. J.M.C acknowledges support from Vinnova (Project ID: 2019-

02878). J.M.C. and N.A.M acknowledge the Center for Nanostructured Graphene, sponsored by the Danish National Research Foundation (Project No. DNRF103). N.A.M. is a VILLUM Investigator supported by VILLUM FONDEN (grant no. 16498). The Center for Nano Optics is financially supported by the University of Southern Denmark (SDU 2020 funding). Simulations were supported by the DeIC National HPC Centre, SDU. J.E.S. thanks support by the European Structural and Investment funds in the FEDER component (Funding Reference: POCI-01-0247-FEDER-033566) and the Portuguese Foundation for Science and Technology FCT (Project number UID/FIS/04650/2019).

Supplementary Information

Detection of the missing cascaded Magneto-Chiral Anisotropy

José M. Caridad[1,2,3], Christos Tserkezis[4], Jaime E. Santos[5], Paulina Plochocka[6], M. Venkatesan[1], J.M.D. Coey[1], N. Asger Mortensen[3,4,7], Geert L.J.A. Rikken[6] and Vojislav Krstić[1,8]

[1]*School of Physics, CRANN, Amber Research Centre, Trinity College Dublin, College Green, Dublin 2, Ireland*

[2]*DTU Physics, Technical University of Denmark, 2800 Kongens Lyngby, Denmark*

[3]*Center for Nanostructured Graphene, Technical University of Denmark, 2800 Kongens Lyngby, Denmark*

[4]*Center for Nano Optics, University of Southern Denmark, Campusvej 55 DK-5230 Odense, Denmark*

[5]*Centro de Física, Universidade do Minho, P-4710-057 Braga, Portugal*

[6]*Laboratoire National des Champs Magnétiques Intenses, UPR3228 CNRS/INSA/UGA/UPS, Toulouse and Grenoble, France*

[7]*Danish Institute for Advanced Study, University of Southern Denmark, Campusvej 55 DK-5230 Odense, Denmark*

[8]*Department of Physics, Friedrich-Alexander-University Erlangen-Nürnberg (FAU), Staudtstr. 7, 91058 Erlangen, Germany*

S1. Axial wave propagation along the helical axis of periodic helical media in the presence of cascaded MChA and pure MChA effects. Reflectance calculation.

It is possible to obtain an analytic expression for the dispersion relation of periodic (biaxial) helical media in the case of the wave propagation $\boldsymbol{k}$ parallel to the helical axis[S1-S4] (here situated along the z direction in Cartesian coordinates for convenience) and $\boldsymbol{B}$.

In general, these periodically inhomogeneous media are characterized by the dielectric tensor shown in Eq.4, main text, re-written here for convenience:

$$\varepsilon(z)=\varepsilon_m\cdot\begin{pmatrix} 1+\delta_\varepsilon\cos(2az) & \delta_\varepsilon\sin(2az)+\dfrac{i\beta|\boldsymbol{B}|\cos\theta}{\varepsilon_m} & 0 \\ \delta_\varepsilon\sin(2az)-\dfrac{i\beta|\boldsymbol{B}|\cos\theta}{\varepsilon_m} & 1-\delta_\varepsilon\cos(2az) & 0 \\ 0 & 0 & 1-\delta_\varepsilon \end{pmatrix}, \quad \text{(Eq. S1)}$$

with $\varepsilon_m=(\varepsilon_1+\varepsilon_2)/2$, $\varepsilon_1,\varepsilon_2$ are the principal axis of the dielectric constant tensor in a coordinate frame (x',y',z) (local to the structure) that rotates with respect to the Cartesian laboratory coordinate frame (x,y,z). In this expression, $\beta|\boldsymbol{B}|$ is the MOA, and the NOA of the system is reflected in the parameter $a=2\pi/p_0$, where p_0 is the pitch of the helix in the absence of a magnetic field. θ is the angle between the propagation direction of waves with wavevector $\boldsymbol{k}$ and the magnetic field $\boldsymbol{B}$ direction ($\cos\theta=\pm1$ for the here considered propagation cases along the helical axis) . Importantly, contrary to naturally gyrotropic systems, the NOA activity in artificial helical media such as our ferromagnetic nanohelices is exclusively caused by the twisting of the medium[S1-S4] and is characterized by a coefficient $\alpha=ca/(\omega\sqrt{\varepsilon_m})=\lambda/(p_0\sqrt{\varepsilon_m})$, where ω is the angular frequency of the incident wave and c is the speed of light. The problem of light propagation in these media is solved representing the fields in the medium in two circular components [S1-S4]. We consider the case of a permeability tensor equal to the unit matrix $\mu=I$ and a non-absorbing medium for simplicity, but the problem can also be addressed in the general case $\mu\neq I$ [S2,S4] and in the presence of absorption[S1,S4].

The dispersion relation for these systems is given by [S2-S4] :

$$b^4 + a_1 b^2 + a_2 b + a_3 = 0 \quad \text{(Eq. S2)}$$

where $a_1 = -2(1+\alpha^2)$, $a_2 = 4\alpha\beta|\boldsymbol{B}|\cos\theta/\varepsilon_m$, $a_3 = -2\alpha^2 + (1-\delta_\varepsilon - \beta|\boldsymbol{B}|\cos\theta/\varepsilon_m)$. The exact roots of equation S2, b_j, can be found in Ref S2 and are the one we use for the calculations in Figure S1. Nevertheless, for simplicity, we mention here the approximated solution of this equation: roots of Eq. S2 can be approximated to[S1] $b_j \approx b_j^0 + (\alpha\beta|\boldsymbol{B}|\cos\theta)/\psi$, where b_j^0 are the roots of the equation when $\alpha = 0$ or $\beta = 0$ and ψ is a parameter of the system containing the principal axes of the permittivity tensor $\varepsilon_1, \varepsilon_2$ and the light wavelength[S1].

Since the roots b_j are related to the wavevector of the circular components of the field $\boldsymbol{k}^\pm$ as $\boldsymbol{k}^\pm = b_j \pm \alpha$; $\boldsymbol{k}^\pm$ can be then approximated by $\boldsymbol{k}^\pm \approx \boldsymbol{k}_0^\pm + (\alpha\beta|\boldsymbol{B}|\cos\theta)/\psi$, where $\boldsymbol{k}_0^\pm$ is the wavevector of the medium when $\alpha = 0$ or $\beta = 0$.

In the following, we point out the main differences in the dispersion relation and wave propagation for the following specific cases:

i) When only the cascaded MChA effect is present (i.e. $\gamma = 0; \beta \neq 0$)

ii) When only the pure MChA effect is present (i.e. $\gamma \neq 0$; $\beta = 0$)

iii) When both pure and cascaded MChA effects are present (i.e. $\gamma \neq 0$; $\beta \neq 0$)

In particular, we highlight the unique wavelength dependency of the cascaded MChA in helical systems, main effect of the present study. We note that the odd-power product $a_2\boldsymbol{k} = 4\alpha\beta|\boldsymbol{B}||\boldsymbol{k}|\cos\theta/\varepsilon_m$ in Eq.S2 (term containing $\Delta = \alpha\beta\boldsymbol{B}\cdot\boldsymbol{k}$ main text, Eq.1) is the key factor to understand the existing differences between all these cases: it represents the origin of the cascaded effect and the non-reciprocal optical properties for forward and backward

propagation in ferromagnetic helical media [S1,S3]. Finally, we justify why our measured ΔR is univocally due to the cascaded MChA effect (case *i)*).

Case *i)*

The term a_2 breaks both parity and time reversal symmetry and generates the cascaded ($\alpha\beta$) MChA effect in the system. The existence of this term is directly related to the presence of both NOA α and MOA β, and gives rise to anisotropies in the optical properties (transmission, reflection, absorption) in these systems[S1-S4]. We note that, for a fixed $\boldsymbol{B}$, the magnitude for forward and backward wave vectors is different when the cascaded effect is present ($|\boldsymbol{k}_f| \neq |\boldsymbol{k}_b|$), i.e. $\boldsymbol{k}_f$ and $\boldsymbol{k}_b$ are not simultaneous solutions of the system[S1-S4]. Moreover, in the presence of $\Delta = \alpha\beta\boldsymbol{B}\boldsymbol{k}$, the optical properties of the film are highly different for $+|\boldsymbol{B}|$ and $-|\boldsymbol{B}|$, even at qualitative level (see for instance the reflectance in Figure S1a). In this sense, the transmission $\Delta T = T(+|\boldsymbol{B}|) - T(-|\boldsymbol{B}|)$ and reflectance differences $\Delta R = R(+|\boldsymbol{B}|) - R(-|\boldsymbol{B}|)$ for polarized light traversing the media do not vanish[S1,S3] and show a zero-crossing at the NOA resonance (unique wavelength position where $|\boldsymbol{k}_f| = |\boldsymbol{k}_b|$) and a sign reversal for the two enantiomers of the system[S1-S4] . This behaviour can be seen below in Figure S1b where ΔR is calculated as a function of the wavelength. Importantly, despite ΔR only accounting for the cascaded MChA effect in Figure S1, its wavelength dependence is qualitatively similar to the one numerically calculated for our ferromagnetic helical nanostructures (Figure 2b in the main text). This qualitative agreement occurs despite no assumptions are made for α, β and/or γ in our numerical simulations and demonstrates that the cascaded MChA effect is the mechanism giving rise to the measured ΔR in our nanohelices (Figure 3b, main text).

Case *ii)*

A different scenario occurs when only the pure MChA effect is present ($\gamma \neq 0$; $\beta = 0$) in helical systems. We note that the pure MChA effect can be accounted for by the alteration of α (NOA) due to the presence of an external magnetic field the system[S4,S5]: i.e. $\alpha' = \alpha + \gamma |\boldsymbol{B}| \cos\theta$. This implies that, up to a first approximation, the pure MChA effect in helical media is a direct consequence of perturbations to the helical pitch[S1,S2,S4] p_0 due to the presence of the external magnetic field $\boldsymbol{B}$.

In this case, the term $a_2 = 4\alpha\beta|\boldsymbol{B}|\cos\theta/\varepsilon_m$ does not exist (β =0), and Eq.S2 can be simplified to a biquadratic expression:

$$b^4 + a_1 b^2 + a_3 = 0 \quad \text{(Eq. S3)}$$

Following Eq.S3, we first note that the remaining coefficients (a_1, a_3) containing the term $\alpha'^2 = \alpha^2 + \gamma^2 |\boldsymbol{B}|^2 \cos^2\theta + 2\alpha\gamma|\boldsymbol{B}|\cos\theta$ do not simultaneously break parity and time reversal symmetry. Furthermore, the roots of Eq.S3 for forward and backward propagation $\boldsymbol{k}_f$ and $\boldsymbol{k}_b$ will only show a comparably small change in the absolute value of α'^2 in this case, given by the third order term $2\alpha\gamma|\boldsymbol{B}|$.This means that $|\boldsymbol{k}_f| = |\boldsymbol{k}_b|$ in this system up to a second order approximation, i.e. the system is reciprocal up to that order when $\gamma \neq 0$; $\beta = 0$.

Finally, we note that, first, contrary to the cascaded effect, reflectance $R(+|\boldsymbol{B}|)$ and $R(-|\boldsymbol{B}|)$ due to the pure effect are qualitatively similar to the one at zero field $R(0)$ (see Figure S1c): they will only show a shift in wavelength due to the distortion of p_0 in the presence of $\boldsymbol{B}$. Second, the reflectance difference $\Delta R = R(+|\boldsymbol{B}|) - R(-|\boldsymbol{B}|)$ does not show a zero-crossing at the NOA resonance due to the pure effect (Figure S1d) as in the cascaded MChA. The absence of a zero-crossing at the NOA due to the pure effect has been already experimentally seen in helical (and non-ferromagnetic) *liquid* crystals[S6].

The magnitude of ΔR related to the pure effect contribution in these systems will thus depend on the degree of distortion of the helical pitch p_0 by the external magnetic field in these systems. Being our nanohelices in a solid state, and having performed our magneto-optical measurements at low magnetic fields (< 0.4 T), the pitch our helices will not be severely modified and thus the contribution to the reflectance by the pure effect in our samples will be $\Delta R \sim 0$. We note that this fact is supported by the small magnetostriction effects observed in nickel at ~0.1T (~0.002%[S7]). Furthermore, this agrees with our numerical calculations (Fig.2, main text) not displaying the predicted features of the pure effect: the helical pitch was kept constant at p_0 in all calculations (i.e. even in the presence of an external magnetic field).

Case *iii)*

Even if both cascaded and pure MChA effects are present in the system, one can show that the cascaded MChA effect dominates the reflectance of ferromagnetic helical nanostructures over the pure MChA effect. Regarding the dispersion relation, the term $a_2|\boldsymbol{k}|$ in this case is proportional to $\beta|\boldsymbol{B}|\alpha'|\boldsymbol{k}| = \beta\alpha|\boldsymbol{B}||\boldsymbol{k}|\cos\theta + \beta\gamma|\boldsymbol{B}|^2|\boldsymbol{k}|\cos^2\theta$. The first term is the origin of the cascaded MChA (case *i)* above); while the second term in this expression (term containing γ) is a new (third order) term which does not simultaneously break parity and time reversal symmetries. Moreover, since $\beta\gamma|\boldsymbol{B}|^2|\boldsymbol{k}|\cos^2\theta$ does not break time reversal symmetry, this term does not contribute to the reflectance difference $\Delta R(\pm|\boldsymbol{B}|)$.

Also, we note that the second order term $\beta\alpha|\boldsymbol{B}||\boldsymbol{k}|\cos\theta$ governs the magneto-optical response of helical nanostructures with respect to the third order term $\beta\gamma|\boldsymbol{B}|^2|\boldsymbol{k}|\cos^2\theta$.

Finally, for completeness, we emphasize that the cascaded MChA effect can only be univocally detected in helical media in reflection but not in transmission: additional magneto-optical phenomena are predicted to occur in these systems in transmission if the constituting material has losses[S4] as in our case (nickel). This is also confirmed in our numerical calculations below, showing a clearly different dependence of the transmission difference ΔT on the wavelength λ with respect to $\Delta R(\lambda)$ (Figure 2 main text).

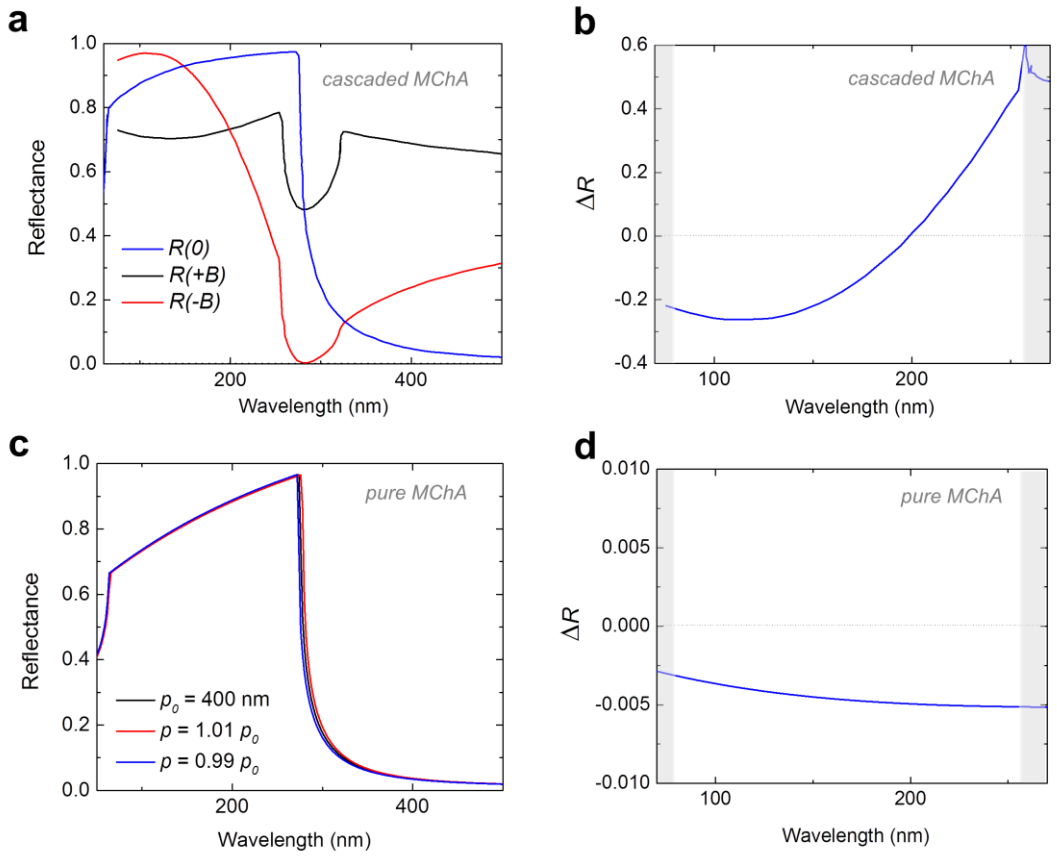

Figure S1. ***Reflectance difference calculation*** $\Delta R = R(+|\boldsymbol{B}|) - R(-|\boldsymbol{B}|)$ at an interface between vacuum and semi-infinite right-handed helical media with pitch p_0 = 400 nm, $\varepsilon_m = 0.25$ and $\delta_\varepsilon = 0.9$ (same parameters as in Ref. S2), accounting for cascaded (a,b) and pure (c,d) MChA effects. **a,** Reflectance of helical media due to the cascaded MChA, depending on the

wavelength λ in the absence (blue) and presence (red, black) of an external magnetic field $|\boldsymbol{B}|$ aligned to the helical axis. At zero field, we have considered right-handed circularly polarized light to calculate the $R(0)$. From this graph, one can see that the NOA region in this system lies between 70 - 300 nm (around the wavelength $\lambda \sim p_0\sqrt{\varepsilon_m}$ = 200 nm). In the presence of magnetic field, incident light considered in the calculations is linearly polarized along the *x* direction. For these calculations the value of the field is such that the MOA parameter of the system is $\beta|\boldsymbol{B}| = +0.25$ or $\beta|\boldsymbol{B}| = -0.25$ (red and blue cases, respectively). **b**, Calculated reflectance difference $\Delta R = R(+|\boldsymbol{B}|) - R(-|\boldsymbol{B}|)$ of the helical system extracted from panel a. A clear zero-crossing occurs within the NOA resonance of the system (non-shadowed part) at the NOA wavelength ~ $p_0\sqrt{\varepsilon_m}$ =200 nm. We only consider a semi-infinite helical medium for simplicity, however, similar behaviour occurs when considering a slab of helical media[S2,S4]. **c,** Reflectance of helical media due to the pure MChA depending on the wavelength λ in the absence (black) and presence (red, blue) of an external magnetic field $|\boldsymbol{B}|$ aligned to the helical axis (accounted for as a 1% perturbation of the helical pitch p_0). Here, we have considered right-handed circularly polarized light to calculate these reflectances. **d**, Calculated reflectance difference $\Delta R = R(+|\boldsymbol{B}|) - R(-|\boldsymbol{B}|)$ of the helical system extracted from panel c. No zero-crossing occurs within the NOA resonance of the system (non-shadowed part) when only accounting for the pure MChA. Finally, we note that more realistic perturbations of p_0, such as the actual magnetostriction effects in nickel (0.002% at ~0.1T[S7]) would produce $\Delta R \sim 0$ in these helical systems.

S2. Magnetic characterization of the samples under study

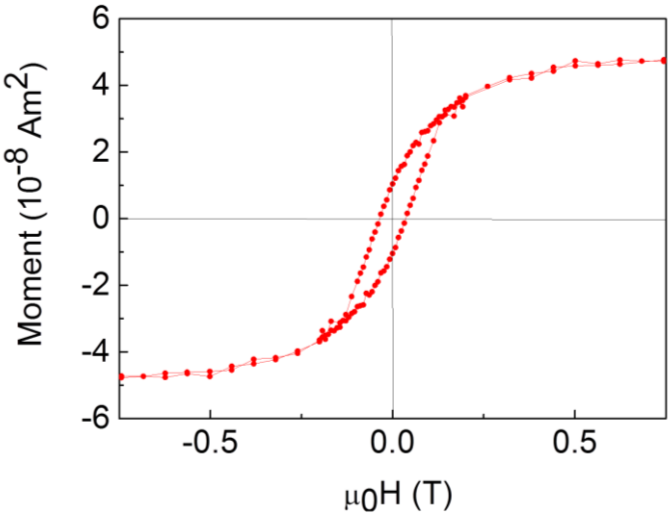

Figure S2. Magnetic characterization of the samples under study. Magnetization curve with field applied parallel to the axis of the nanohelices shown in (Figure 1b) measured with a SQUID magnetometer. Their saturation for these samples is produced at an external field ~0.4 T. The latter agrees with an increasing $|\eta|$ observed in the magneto-optical response of our samples when increasing the external magnetic field below saturation (Supplementary Note 4).

S3. Simulated magneto-optical activity of nickel nanohelices in transmission

Additional magnetochiral effects other than the cascaded effect may occur in transmission[S1,S2,S4], so the transmission difference $\tau = (T(\boldsymbol{B}) - T(-\boldsymbol{B})) \cdot T(0)^{-1} \cdot |\boldsymbol{B}|^{-1}$ in helical

media normalized with respect to the magnetic field ***B*** and the transmission at zero field $T(0)$ might *i)* have a different wavelength dependence from the one shown at normal reflection $\eta(\lambda)$ and *ii)* have a different magnitude than $\eta(\lambda)$.

Indeed, the calculated $\tau(\lambda)$ does not show any zero-crossing around the NOA resonance λ^{max} (wavelength range 650 ± 25 nm, Figure S3) in clear contrast to the optical magneto-chiral response calculated in normal reflection $\eta(\lambda)$ (Figure 3b, main text). Instead, $\tau(\lambda)$ shows a maximum close to λ^{max} in agreement with the fact that additional contributions other than the cascaded effect affect the transmission difference of this system[S4]. This is additionally confirmed by noticing that $\tau(\lambda)$ is ~10^{-4} T^{-1}, one order of magnitude larger than $\eta(\lambda)$.

For completeness, we note that the MChA signal measured in transmission similar type of samples[S8] agrees well with our calculations: it does not show any zero-crossing close to the NOA maximum (650 ± 25 nm) and its magnitude is ~10^{-4} T^{-1}, too. Furthermore, the overall lineshape is similar $\tau(\lambda)$. Slight differences between our calculated τ (Figure S3) and the measured MChA signal in transmission in Ref.[S8] at different wavelengths are attributed to the considerable differences in the size of helices in both studies (our samples have a pitch of ~320 nm, whereas samples in Ref. [S8] have a pitch of ~50 nm).

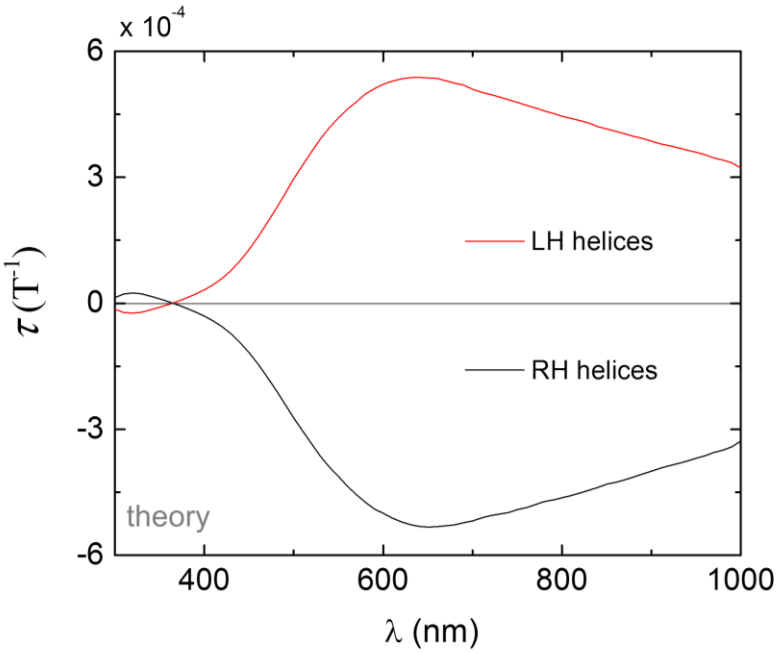

Figure S3. Calculated normalized MChA signal in transmission $\tau = (T(\boldsymbol{B}) - T(-\boldsymbol{B})) \cdot T(0)^{-1} \cdot |\boldsymbol{B}|^{-1}$ of both RH and LH helices plotted as a function of the laser wavelengths. In the former expression $\tau(0)^{-1}$ is the transmission signal at zero magnetic field. We note that this magneto-optical signal may contain, in principle, several MChA effects[S4], making thus the wavelength dependence of $\tau(\lambda)$ and that one for the cascaded MChA $\eta(\lambda)$ different. Indeed, contrary to $\eta(\lambda)$, no zero-crossing is observed within the NOA resonance range (650 ± 25 nm) in $\tau(\lambda)$.

S4. Variation of $|\eta|$ with B

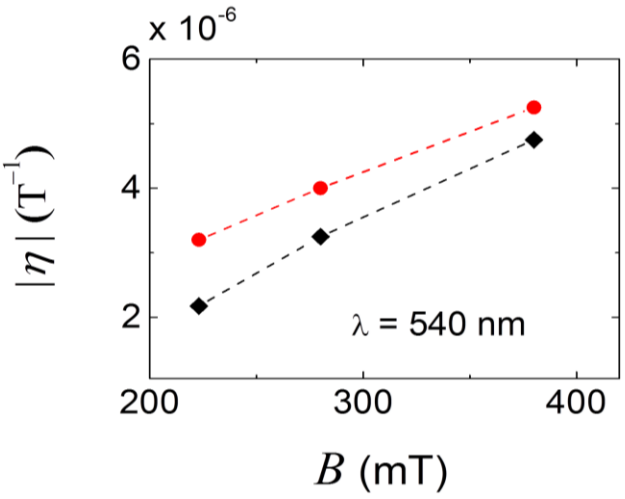

Figure S4. Magnitude of η for the samples under study LH helices (red) and RH helices (black) for different external magnetic fields ***B*** at an excitation wavelength of 540 nm. $|\eta|$ increases linearly when increasing the external magnetic field ***B*** . We do not observe a saturation of the signal since the maximum magnetic field used in these measurements is below the saturation field of our samples (see Figure S2).

S5. Magnetic optical activity of nickel nanohelices

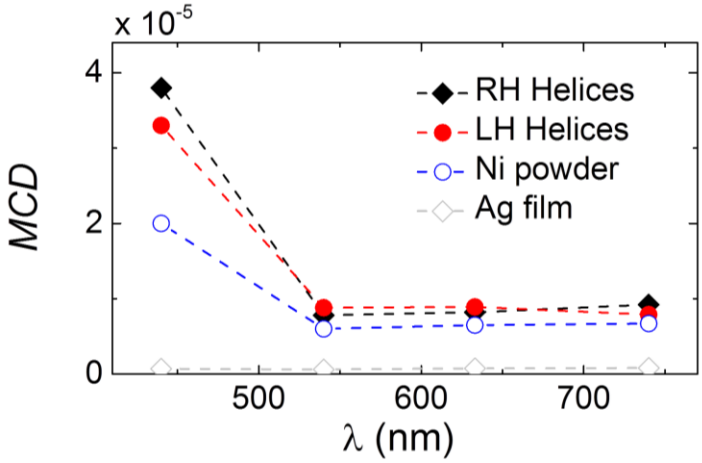

Figure S5. Measured MOA (magnetic circular dichroism MCD) of our samples extracted as the difference $R^{RHCP} - R^{LHCP}$ at an external magnetic field $\boldsymbol{B}$ = 0.375T and different laser wavelengths. Measurements of MCD on our substrate (Ag thin film, grey) show a much smaller signal than the one of nickel nanohelices and nickel powder (blue), indicating that the MOA activity is indeed higher in ferromagnetic materials. Not only that, our data also shows a larger MCD signal in our nanohelices than in (micron size) nickel (Ni) powder. This behaviour may be due to the plasmonic activity of Ni nanohelices in the measured wavelength range[S9], situation already observed in other nanostructures[S10]. Finally, we note that this signal manifests the MOA of the system, having thus an estimated normalized parameter $\beta \sim 1\times10^{-4}$ T^{-1}.

S6. Further description of the theoretical calculations

We provide additional information regarding the finite-element simulations in this section. Figure S6 shows the simulation setup, implemented in Comsol Multiphysics 5.1, RF module. Figure S6a shows the full simulation area. The unit cell is a cuboid with sides equal to 200 nm (*x* and *y* directions) and 750 nm (*z* direction). A nickel helix with major radius 75 nm, minor

radius 45 nm, pitch 300 nm, 1 turn, and rotated by 30 degrees with respect to the z axis, is placed in the unit cell (air), over a 250 nm-thick silver substrate described by its experimental dielectric function[S11] . A perfectly-matched layer (PML, 500 nm thick) boundary condition is used on top of the simulation area, while a scattering boundary condition is used below the Ag substrate. The system is illuminated by a port placed at the PML/air interface, either linearly or circularly polarized. Reflectance and transmittance spectra are calculated by integrating energy flow over the PML/air interface and the end face of the Ag substrate, respectively, as noted in Figure S6a.

Since the dimensions of the helix in the *x*-*y* plane exceed the unit cell, it is necessary to split the helix into smaller parts, as shown in Figure S6b for a right-handed helix. Four helices are placed at the four corners of the unit cell, and the parts that lie outside the unit cell are then subtracted. This means that appropriate Floquet boundary conditions need to be applied to the faces of the helix that intersect the unit cell boundaries. The same procedure is followed for left-handed helices.

For the transmittance simulations, the Ag substrate is replaced by a glass substrate with dielectric function equal to 2.1, followed by a 500 nm-thick PML. The transmittance integration then takes place at the glass/PML interface.

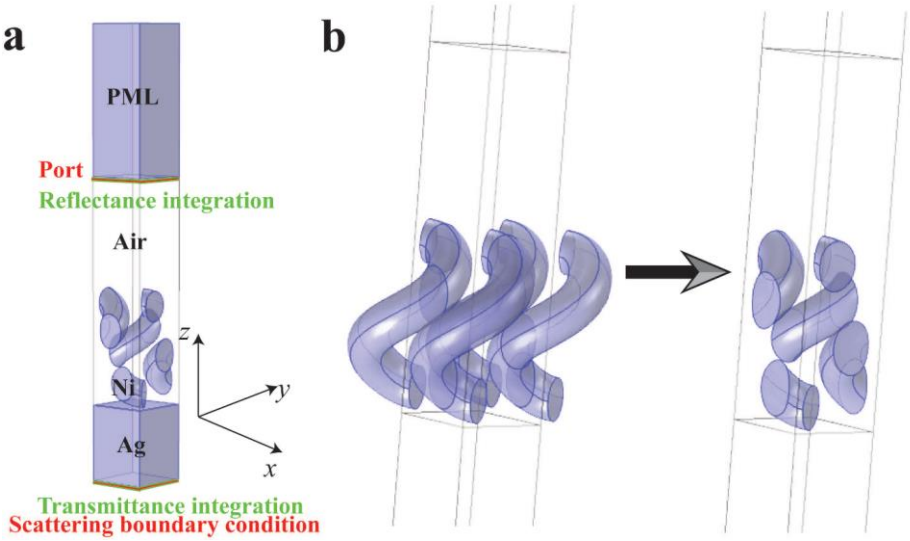

Figure S6. **a**, full view of the simulation area. **b** Parts of 4 helices are used to reduce the lattice constant (i.e. separation between helices).

Regarding the permittivity of Ni in the presence of a static magnetic field, we use the fitting to experimental data from Ref. S12. The permittivity tensor is related to the susceptibility tensor through $\bar{\varepsilon} = 1 + \bar{\chi}$, and it contains a retarded Drude contribution plus two Lorentzians for the diagonal elements, and a sum of Lorentzians for the non-diagonal elements, as follows (the magnetic field is assumed along the z direction):

$$\chi(\omega) = \begin{pmatrix} \chi_{xx} & \chi_{xy} & 0 \\ \chi_{yx} & \chi_{yy} & 0 \\ 0 & 0 & \chi_{zz} \end{pmatrix} \quad \text{Eq. S4}$$

where

$$\chi_{xx} = \chi_{yy} = -\overbrace{\frac{\omega_p^2(\omega+i\gamma_D)(1-i\omega\tau_D)}{\omega[(\omega+i\gamma_D)^2-\Omega_{cD}^2]}}^{\text{retarded Drude}} - \sum_{i=1}^{2} \overbrace{\frac{\Delta_{Li}\omega_{Li}^2(\omega^2+i\omega\gamma_{Li}-\omega_{Li}^2)}{(\omega^2+i\omega\gamma_{Li}-\omega_{Li}^2)^2-\omega^2\Omega_{ci}^2}}^{\text{Lorentzians}} \quad \text{Eq.S5}$$

$$\chi_{xy} = -\chi_{yx} = \overbrace{\frac{i\omega_p^2\Omega_{cD}(1-i\omega\tau_D)}{\omega[(\omega+i\gamma_D)^2-\Omega_{cD}^2]}}^{\text{retarded Drude}} - \sum_{i=1}^{2} \overbrace{\frac{i\,\Delta_{Li}\omega_{Li}^2\omega\Omega_{ci}}{(\omega^2+i\omega\gamma_{Li}-\omega_{Li}^2)^2-\omega^2\Omega_{ci}^2}}^{\text{Lorentzians}} \quad \text{Eq.S6}$$

$$\chi_{zz} = \overbrace{-\frac{\omega_p^2(1-i\omega\tau_D)}{\omega(\omega+i\gamma_D)}}^{\text{retarded Drude}} + \sum_{i=1}^{2} \overbrace{\frac{\Delta_{Li}\omega_{Li}^2}{(\omega_{Li}^2-i\omega\gamma_{Li}-\omega^2)}}^{\text{Lorentzians}} \quad \text{Eq.S7}$$

The parameter values used are[S13]:

$\hbar\omega_p = 6.07$ eV, $\hbar\gamma_D = 0.0305$ eV, $\hbar/\tau_D = 4.55$ eV, and $\hbar\Omega_{cD} = 0.0499$ eV for the plasma frequency, the damping rate, the retardation time and the cyclotron frequency in the Drude model, respectively;

$\hbar\omega_{L1} = 0.918$ eV, $\hbar\gamma_{L1} = 2.66$ eV, $\Delta_{L1} = 93.1$, and $\hbar\Omega_{cL2} = 0.0204$ eV for the Lorentz frequency, the Lorentz damping rate, the oscillator strength and the cyclotron frequency in the first Lorentz model, respectively;

$\hbar\omega_{L2} = 4.62$ eV, $\hbar\gamma_{L2} = 1.62$ eV, $\Delta_{L2} = 2.32$, and $\hbar\Omega_{cL2} = -0.0312$ eV for the Lorentz frequency, the Lorentz damping rate, the oscillator strength and the cyclotron frequency in the second Lorentz model, respectively.

We note that the cyclotron frequency Ω_{cD} corresponds to a magnetic field B between 85 and 95 T (through $\Omega_{cD} = \frac{e}{m}B$ where $-e$ is the electron charge and m its effective mass), assuming an effective mass of about 1/5 to 1/4 the electron mass[S13,S14]. We have used B = 90 T to normalize the calculated $\eta(\lambda)$ and $\tau(\lambda)$ (Figure 3, main text; and Figure S3).

Supplementary References

S1. O.S.Eritsyan. Time dispersion, waves irreversibility and absorption effects in cholesteric liquid crystals. Mol. Cryst. Liq. Cryst. **348**, 79-99 (2000)

S2. A.H. Gevorgyan. Magneto-optics of a thin film layer with helical structure and enormous anisotropy. Mol. Cryst. Liq. Cryst. **382**, 1-19 (2010)

S3. I. Bita and E.L. Thomas. Structurally chiral photonic crystals with magneto-optic activity: indirect photonic bandgaps, negative refraction and superprism effects. J. Opt. Soc. Am. B. 22, 6, 1199 (2005)

S4. A.H. Gevorgyan and G.A. Vardanyan. Nonreciprocal reflection at the presence of absorption. Proc. SPIE 5218, Complex Mediums IV: Beyond Linear Isotropic Dielectrics, (9 July 2003); https://doi.org/10.1117/12.507791

S5. G.J.L.A. Rikken and E. Raupach. Pure and cascaded magnetochiral anisotropy in optical absorption. Phys. Rev. E 58, 5081 (1998)

S6. C.Koerdt, G. Düchs and G.L.J.A. Rikken. Magnetochiral anisotropy in Bragg scattering. Phys. Rev. Lett. 91, 7, 073902 (2003)

S7. P. Mc Corkle. Magnetostriction and magnetoelectric effect in Iron, Nickel and Cobalt. Phys. Rev. 22, 271 (1923).

S8. S. Eslami, J.G. Gibbs, Y. Rechkemmer, J. v Slageren, M. Alarcón-Correa, T-C. Lee, A.G. Mark, G.L.J.A. Rikken and P. Fischer. Chiral nanomagnets. ACS Photonics, 1, 1231 (2014).

S9. J. M. Caridad, D. McCloskey, F. Rossella, V. Bellani, J.F. Donegan and V. Krstić. Effective Wavelength scaling of and damping in plasmonic helical antennae. ACS Photonics **2**, 675-679 (2015).

S10. J.B. González-Díaz, A. García-Martín, G. Armelles, D. Navas, M. Vázquez, K. Nielsh, R.B. Wehrspohn and U. Gösele. Enhanced magneto-optics and size effects in ferromagnetic nanowire arrays. Adv. Mater. **19**, 2643 (2007).

S11. P.B. Johnson, R.W. Christy. Optical constants of the noble metals. Phys. Rev. B **6**, 4370 (1972).

S12. C. Wolff, R. Rodríguez-Oliveros, K. Busch. Simple magneto-optic transition metal models for time-domain simulations. Opt. Express **21**, 12022-12037 (2013).

S13. J. W. D. Connolly. Energy bands in ferromagnetic nickel. Phys. Rev. **159**, 415-426 (1967).

S14. D. C. Tsui. De Haas-van Alphen effect and electronic band structure of nickel. Phys. Rev. **164**, 669-683 (1967).